Forward-angle inelastic scattering

G. F. Bertsch and O. Scholten

Cyclotron Laboratory, Michigan State University, East Lansing, Michigan 48824
and Institute for Theoretical Physics, University of California at Santa Barbara,
Santa Barbara, California 93106
(Received 28 September 1981)

The single-step contribution to nuclear inelastic scattering is analyzed in the independent particle model. We derive simple formulas for the single-step total cross section and the response function, which are the two major ingredients in the theory. This description accounts for most of the cross section below an excitation energy of 40 MeV, seen in proton induced reactions at 200 and 800 MeV.

NUCLEAR REACTIONS Calculated proton induced one step continuum $\sigma(E,E_p)$, $q(E,E_n)$, $\sigma(\theta)$ at 200 and 800 MeV protons.

I. INTRODUCTION

Inelastic scattering reactions are particularly interesting at forward angles because the low momentum transfer probes the collective response of nuclei to external fields. However, the collective cross section is obscured by a background which we would like to understand better. One question is whether this background arises primarily from single or multiple collisions. In this work we will examine the single step contribution to the cross section. We consider the regime of excitation energies below 40 MeV in proton-induced reactions with proton energy greater than 200 MeV, and we will show that the single step contribution accounts for most of the cross section at momentum transfers larger than 0.5 fm^{-1}. The inclusive inelastic scattering has been previously studied by Chiang and Hüfner.[1] Our approach is similar in spirit to this work.

The theory of the cross section will be based on the distorted-wave impulse approximation which allows the nucleon-nucleon cross section to be factorized from the nuclear response.[2] We express the cross section in the form

$$\frac{d^2\sigma}{d\Omega\,dE} = \frac{d\sigma}{d\Omega}\bigg|_{NN} N_{\text{eff}}S(q,E) . \qquad (1.1)$$

Here $d\sigma/d\Omega\,|_{NN}$ is the nucleon-nucleon cross section at the same laboratory energy and angle. The second factor in this equation, N_{eff}, is the effective number of target particles which will be discussed

in Sec. II. The nuclear response to the projectile scattering probe is $S(q,E)$. This is defined by

$$S(q,E) = \frac{\displaystyle\sum_{i,f} \langle \psi_i \mid \mathscr{O}_q \mid \psi_f \rangle^2 \delta(E_f - E_i - E)}{\displaystyle\sum_i \langle \psi_i \mid \mathscr{O}_q^* \mathscr{O}_q \mid \psi_i \rangle} , \qquad (1.2)$$

where $\mathscr{O}_q$ is the projectile scattering operator, and ψ_i and ψ_f are occupied and unoccupied single-particle states. Note that in the limit that $\mathscr{O}_q \mid \psi_i \rangle$ orthogonal to all the $\mid \psi_{i'} \rangle$ (no Pauli blocking), S satisfies

$$\int dE\, S(q,E) = 1 . \qquad (1.3)$$

We discuss the theory of $S(q,E)$ in Secs. III and IV. In Sec. III we review the Fermi gas model for the response, which is used in Ref. 1. Our main interest is the small momentum transfers, which requires a better treatment of the nuclear surface than is possible in the Fermi gas model. We present the theory of S in a semi-infinite slab model in Sec. IV. Finally, in Sec. V we present a detailed comparison of these models with proton-induced reactions at 200 and 800 MeV.

II. SINGLE STEP TOTAL CROSS SECTION

We define the cross section $\sigma^{(n)}$ for n collisions between projectile and target particles in the nucleus. The effective number of nucleons participat-

ing in one-step reactions is then given by

$$N_{\text{eff}} = \frac{\sigma^{(1)}}{\sigma_{NN}} , \qquad (2.1)$$

where σ_{NN} is the nucleon cross section used to calculate the single step reaction cross section $\sigma^{(1)}$. In the Glauber theory, $\sigma^{(n)}$ is given by

$$\sigma^{(n)} = \int d^2b \frac{[\mathcal{X}(b)]^n}{n!} e^{-\mathcal{X}(b)} , \qquad (2.2)$$

where $\exp[-\mathcal{X}(b)]$ is the attenuation factor and

$$\mathcal{X}(b) = \int dz\, \rho(r = \sqrt{z^2 + b^2})\sigma_{NN} \qquad (2.3)$$

is the average number of collisions as a function of the impact parameter b. We will parametrize the nuclear density in terms of a Fermi function,

$$\rho(r) = \rho_0 / (1 + e^{(r-R)/a}) \qquad (2.4)$$

using the parameters of Ref. 6.

The inelastic background is primarily due to $\sigma^{(1)}$, and we shall need to evaluate this cross section carefully. It is a simple matter to compute this numerically from Eqs. (2.2)—(2.4). In Fig. 1 we show for one case, ^{208}Pb, the contribution to $\sigma^{(1)}$ as a function of impact parameter. We see that this is very much surface peaked, with the maximum contribution coming from the vicinity of the quarter density point. Numerical values for $\sigma^{(1)}$ for various reactions of interest are tabulated in Table I.

It is useful to estimate $\sigma^{(1)}$ analytically, both for convenient formula, and to exhibit the dependence on the parameters in the calculation. The estimate is easy to obtain in the limit that the main contribution is from the tail of the density distribution. We can then expand the Fermi function to evaluate the integral (2.3).
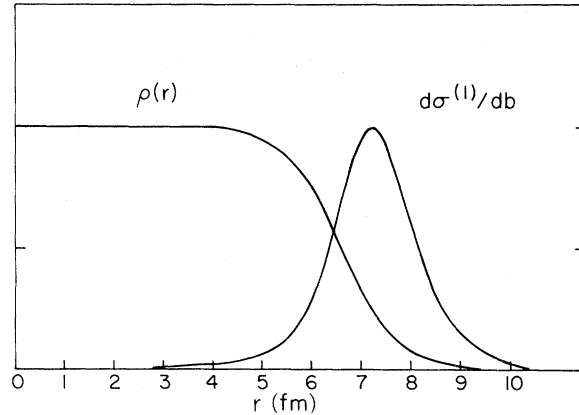

FIG. 1. The density and the contribution to the single step cross section plotted as functions of radius and the impact parameter. The vertical scale has arbitrary units.

$$\mathcal{X}(b) \simeq \int_{-\infty}^{+\infty} dz\, \sigma_{NN}\rho_0 e^{-\sqrt{z^2+b^2}/a + R/a}$$

$$\simeq \int_{-\infty}^{\infty} dz\, \sigma_{NN}\rho_0 e^{(R-b)/a} e^{-z^2/(2ab)}$$

$$= \sigma_{NN}\rho_0 e^{(R-b)/a}\sqrt{2\pi ab} . \qquad (2.5)$$

Since we will need a better accuracy, we expand $\rho(r)$ to second order, giving

$$\mathcal{X}(b) = \sigma_{NN}\rho_0 \sqrt{2\pi ba}\, e^{(R-b)/a}$$

$$\times \left[1 - \frac{1}{\sqrt{2}} e^{(R-b)/a} + \cdots \right]. \qquad (2.6)$$

We are interested in the region $\mathcal{X}(b) \simeq 1$, which is satisfied for the usual nuclear parameters with $b > R$. This latter condition is required for the series expansion to be valid.

We next evaluate the single step scattering cross

TABLE I. Single collision total cross section calculated with $\rho_0 = 0.16$ fm^{-3} and $a = 0.55$ fm.

	σ_{NN} (mb)	b_0 (fm)	$\sigma^{(1)}$ Eq. (2.8) (mb)	$\sigma^{(1)}$ Eq. (2.1) (mb)	N_{eff}
^{40}Ca	40	3.92	176	215	5.4
^{116}Sn	40	5.86	252	305	7.6
^{208}Pb	40	7.13	301	355	8.9
^{90}Zr	25	4.92	243	330	13.2

section $\sigma^{(1)}$ using the approximate formula for $\chi(b)$, Eq. (2.6). In the integral for $\sigma^{(1)}$ we change the integration variable from db to $d\chi$. Neglecting the b dependence of $\chi(b)$ outside of the exponential factors, we have

$$\chi(b)db = a[-1-\chi(b)/(\sigma_{NN}\rho_0 2\sqrt{\pi ab})$$
$$+\cdots]d\chi(b). \quad (2.7)$$

The cross section $\sigma^{(1)}$ then becomes

$$\sigma^{(1)} = \int_0^\infty d^2b\, \chi(b)e^{-\chi(b)}$$
$$\simeq 2\pi b_0 a \int_0^\infty d\chi\,(b)[1+\chi(b)/(\sigma_{NN}\rho_0 2\sqrt{\pi ab_0})$$
$$+\cdots]e^{-\chi(b)}$$
$$\simeq 2\pi b_0 a[1+(\sigma_{NN}\rho_0 2\sqrt{\pi b_0 a})^{-1}+\cdots], \quad (2.8)$$

where again we have neglected the nonexponential b dependence by replacing b by an average value b_0. The parameter b_0 is roughly given by the condition $\chi(b_0)=1$. Note that the dominant term in $\sigma^{(1)}$ depends mainly on the nuclear geometry and only weakly on the nucleon-nucleon cross section.

In Table I the values of $\sigma^{(1)}$ are quoted, calculated numerically from Eqs. (2.1) and (2.2) for parameters relevant to proton scattering at 200 and 800 MeV. We also show the values obtained from the approximate formula Eq. (2.8), which agree to

within 15% with the numerical integration, and is thus useful for simple estimates. With only the first term in Eq. (2.8) the formula is 40% low.

III. THE FERMI GAS MODEL

In the Fermi gas model, the response to the operator $e^{iq\cdot r}$ can be evaluated analytically.[3] The wave functions in Eq. (1.2) are plane waves, which we label by k for the occupied state and k' for the unoccupied state. Momentum and energy conservation reduce the six dimensional integral in Eq. (1.2) as follows

$$S(q,E) \equiv \frac{1}{N}\sum_{kk'}|\langle k|e^{iq\cdot r}|k'\rangle|^2\delta\left[\frac{k^2}{2m}+E-\frac{k'^2}{2m}\right]$$
$$=\frac{3m}{4qk_F^3}\int d^2k_\perp. \quad (3.1)$$

We defined the z axis along the direction of q, and $k_\perp$ labels the xy component of the momentum of the occupied state. The integration over $k_\perp$ in Eq. (3.1) runs over occupied states only, $k_\perp^2 + k_z^2 \leq k_F^2$ for $E + k_z^2 = (q+k_z)^2$ with the additional condition that $k_\perp^2 + (k_z+q)^2 \geq k_F^2$. The evaluation of the integral (3.1) yields the imaginary part of the Lindhard function.[3]

$$S(q,E)=\begin{cases}\dfrac{3m}{4qk_F^3}2mE & \text{if } |2qk_F|>2mE+q^2, \\[2ex] \dfrac{3m}{4qk_F^3}[k_F^2-(\tfrac{1}{2}q^2-mE)^2/q^2] & \text{if } |2qk_F|<2mE+q^2, \\[2ex] 0 & \text{if } (\tfrac{1}{2}q^2-mE)^2>k_F^2q^2.\end{cases} \quad (3.2)$$

Considered as a function of E at a fixed value of q, $S(q,E)$ is nearly triangular for small values of q as shown in Figs. 4 and 6. This is at variance with the data.

The effect of the Pauli principle is to reduce the energy integrated cross section by a factor $P(q)$,

$$P(q)=\int S(q,E)dE,$$

$$=\begin{cases}\dfrac{3}{4}\dfrac{q}{k_F}\left[1-\dfrac{1}{12}\dfrac{q^2}{k_F^2}\right] & \text{if } q\leq 2k_F, \\[2ex] 1 & \text{if } q\geq 2k_F.\end{cases} \quad (3.3)$$

For example, for 800 MeV (p,p') scattering at 4.5° the momentum transfer is about $q=\tfrac{1}{2}k_F$, giving a blocking factor of $P(\tfrac{1}{2}k_F)=0.37$. However, Eq. (3.3) is qualitatively incorrect. It predicts that the total cross section for quasielastic scattering should vary linearly with q in the forward direction and vanish at $q=0$. Much of the data appears to be independent of q in the forward direction. This is particularly obvious in the (p,n) data which extend to zero degrees. The Fermi gas model does not give a good description of the low-momentum transfer response. A better approximation is needed, which explicitly takes into account the nuclear surface.

IV. THE SEMI-INFINITE SLAB MODEL

The most basic effect of the finite nuclear size, the breaking of translational invariance, can be studied in the semi-infinite slab model of the nucleus. Other effects of finite size, for example, associated with interference between amplitudes from different areas of the nucleus, will not be calculable in the slab model. Interference effects will show up as diffraction structure associated with particular shells. While this is important for the excitation of collective states, for the higher inelasticities we consider there appears to be no diffraction structure.

To calculate the response of the semi-infinite slab, we first must define the single-particle wave functions. We take the surface to be at $z = 0$, and choose the wave functions to be eigenstates of the semi-infinite potential well,

$$V(r) = \frac{V_0}{1 + e^{z/a}} \ . \tag{4.1}$$

We take the well parameters as $V_0 = -45$ MeV and $a = 0.75$, following optical potentials for heavy nuclei.

The scattering operator is not simple $e^{iq \cdot r}$ because of the absorption of the projectile in the interior. Most of the one-step reactions take place when the projectile skims along the surface, as we saw in Fig. 1, and it is reasonable to treat the absorption as a cutoff on the operator in the z direction. We take the scattering operator to be

$$\mathscr{O}(q,r) = e^{iq \cdot r}/(1 + e^{(z_0 - z)/a_0})^{1/2} \ . \tag{4.2}$$

This satisfies the condition that the contribution to the scattering vanishes in the interior. The parameters z_0 and a_0 can be determined by requiring that $d\sigma^{(1)}/db = 2\pi b \mathcal{X}(b) e^{-\mathcal{X}(b)}$, discussed in Sec. II, and $|\mathscr{O}(q,r)|^2 \rho(r)$ are proportional in the surface region.

The projectile is assumed to travel along the surface when it interacts via a single-step collision. The region of the nucleus that is important is a ring in the equatorial plane perpendicular to the beam axis. The angle ϕ between the surface and the momentum transfer is just the azimuthal angle at which the projectile strikes the nucleus, and can have any value. We add contributions to the response for different angles ϕ incoherently,

$$S(q,E) = \int_0^{2\pi} \frac{d\phi}{(2\pi)} \int \frac{d^3k \, d^3k'}{(2\pi)^3 (2\pi)^3} |\langle \psi(k,z) | e^{iqz \cos\phi + iqx \sin\phi} \mathscr{O}(z) | \psi(k',z) \rangle|^2$$

$$\times \delta(E_{k'} - E_k - E) / \int d^3k \langle \psi(k,z) | \mathscr{O}^2(z) | \psi(k,z) \rangle \ . \tag{4.3}$$

Momentum is conserved in the perpendicular direction, and this eliminates two of the integrals, say k_x' and k_y'. The k_z' integration is evaluated with the energy-conserving δ function. Nothing in the integrand depends on k_y, so this integral can be evaluated from the limits imposed by the Fermi sphere. We thereby obtain the following expression for the normalized response function

$$S(q,E) = \frac{2m}{\pi^3} \int_0^\pi d\phi \int dk_z dk_x \left\{ \frac{k_F^2 - k_x^2 - k_z^2}{[(k_z')^2 - 2mV_0]} \right\}^{1/2}$$

$$\times \frac{|\langle \psi(k,z) | \mathscr{O}(q,z) | \psi'(k',z) \rangle|^2}{\int_0^{k_F} dk_z (k_F^2 - k_z^2) \langle \psi(k,z) | \mathscr{O}^*(q,z) \mathscr{O}(q,z) | \psi(k,z) \rangle} \ , \tag{4.4}$$

which can be evaluated numerically. In Eq. (4.4) the x and y dependence of the wave functions and operators has been treated analytically. The overlap involved is therefore only an integration over z. The momentum transfer in the z direction is given by $q_z = q \cos\phi$. The momenta $k_{z'}$ of the bound state ψ, and k_z' of the scattering state ψ' are related by energy conservation as

$$k_z'^2 = k_z^2 + k_x^2 + 2m(E + V_0) - (k_x + q \sin\phi)^2 \ . \tag{4.5}$$

The single particle wave functions ψ and ψ', solutions of the Schrödinger equation with the potential (4.1), are normalized to one in the interior. The integral over the occupied states in the numerator of Eq. (4.4) is further restricted by the conditions imposed on k_z', for which we have considered two cases: (i) $k_z'^2 \geq 0$, which corresponds to the knockout process in which the nucleon escapes from the surface, and (ii) $k'^2 \geq 0$, corresponding to the scattering of the knocked on nucleon to unbound states.

V. AN ANALYTIC APPROXIMATION

In comparing with the data, we have calculated the integral (4.4) numerically, but it is also useful to find an approximate analytic solution. Since the scattering process is mainly a surface phenomenon, it is dominated by the least bound occupied states. In the external region the wave functions for these states are given by

$$\psi(k,r)=f(k_z)e^{-\alpha z}e^{i\vec{k}_\perp\cdot\vec{r}_\perp} , \qquad (5.1)$$

where $\alpha=0.7$ fm^{-1} for 10 MeV binding. The prefactor $f(k_z)$ can be parametrized to fit the Woods-Saxon eigenfunctions. The form

$$f(k_z)=Ak_z e^{Bk_z} \qquad (5.2)$$

with $A=0.24$ fm, $B=1.3$ fm, and $\alpha=0.7$ fm^{-1} reproduces the eigenstates at $z=0$, normalizing the states to $1/$fm^3 in the interior. The unoccupied states for the particle-hole excitation we will approximate by plane waves. Since the plane waves form a complete set of states, the Pauli blocking is lost in the approximation. We restore it by assuming that the response can be factorized,

$$S(q,E)=P(q)S_u(q,E) , \qquad (5.3)$$

where $P(q)$ is the blocking factor and S_u is the response calculated with plane wave final states. In general, the blocking factor P also depends on the transferred energy, which is neglected in the present treatment.

We estimate $P(q)$ using

$$P(q)=1-\frac{\sum|\langle\psi_0|\mathcal{O}(q,r)|\psi_0'\rangle|^2}{\sum\langle\psi_0|\mathcal{O}^*(q,r)\mathcal{O}(q,r)|\psi_0\rangle} , \qquad (5.4)$$

where the summation over ψ_0 and ψ_0' runs over occupied states only. For the scattering operator, we replace (4.2) by a step function $\mathcal{O}(q,z)=e^{iqr}\theta(z)$.

Then (5.4) may be evaluated with the wave functions (5.1) and (5.3)
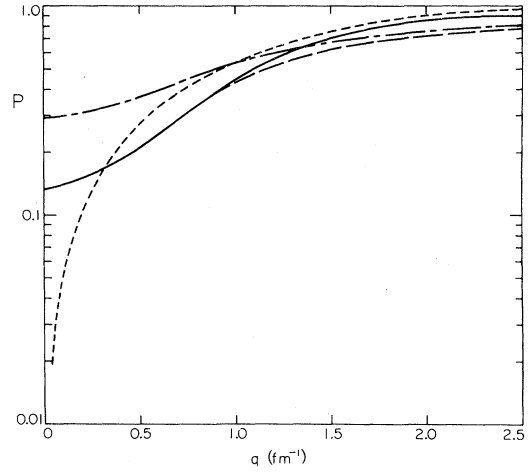
$$P(q)=1-C/(4\alpha^2+q^2) , \qquad (5.5)$$

FIG. 2. The blocking factor as a function of the momentum transfer calculated in different models; the dotted curve gives the blocking calculated in the Fermi gas model, Eq. (3.3); the drawn curve is calculated using Eq. (4.4); the dashed-dotted curve is calculated from (5.5) using Eq. (5.6), while in the dashed curve $C=1.7$ fm^2 has been taken.

$$C=\frac{\alpha A^2}{4\pi B}\left[\exp(2k_FB)\cdot\left[2k_F^2-\frac{2k_F}{B}+\frac{1}{B^2}\right]-\frac{1}{B^2}\right] . \qquad (5.6)$$

In Fig. 2 we compare the blocking factor from Eq. (5.5) with the exact blocking factor obtained by integrating Eq. (4.4) over E. Equation (5.5) is rather inaccurate at $q\approx0$, due to the strong cancellation between the two terms. The dashed curve in Fig. 2, which gives a good fit for $q\leq1$ fm^{-1}, is obtained from (5.5) and (5.6) by increasing C by 15%. The dotted curve is the Fermi gas model. It gives less blocking for $q\geq0.3$ fm^{-1}, and more blocking for $q\leq0.3$ fm^{-1}.

We now consider the plane wave response S_u. This can be written as

$$S_u(q,E)=\frac{\frac{4m\alpha}{\pi^3}\int_0^\pi d\phi\int_0^{k_F}dk_z\int dk_x\frac{f^2(k_z)(k_F^2-k_x^2-k_z^2)^{1/2}}{k_z'[\alpha^2+(k_z'-q\cos\phi)^2]}}{\int_0^{k_F}dk_z(k_F^2-k_z^2)f^2(k_z)} . \qquad (5.7)$$

The limits of the k_x integration are determined by the zeros of k_z' or $(k_F^2-k_z^2-k_x^2)^{1/2}$ in the integrand. Because the integrand behaves quite differently depending on the location of the zeros, it

is difficult to make a rigorous analytic approximation. We arrived at fairly simple formula by considering the two regions separately, and replacing smooth functions in the integrand by average

values. The result is

$$S_u(q,E) = \frac{4m\alpha}{\pi^2[\alpha^2 + (k_0 - q)^2]}$$

$$\times \left[\frac{\phi_0}{k_0} + \frac{(\pi/2) - \phi_0}{3\sqrt{qk_F/2}} \right] , \qquad (5.8)$$

where

$$k_0 = \tfrac{3}{4}k_F^2 + 2m(E + V_0)$$

and

$$\phi_0 = \begin{cases} \pi/2 & \text{if } 2q \leq k_0 , \\ \sin^{-1}(k_0/2q) & \text{if } 2q > k . \end{cases}$$

The range of validity of the approximation is
$E > -V_0 - \tfrac{1}{4}(k_F^2/m)$ and $q \sim k_0$.

VI. COMPARISON WITH EXPERIMENT

A. 800 MeV (p,p')

At 800 MeV the elastic nucleon-nucleon cross section is anisotropic, but can conveniently be parametrized as[4]

$$\frac{d\sigma_{NN}}{d\Omega_{c.m.}} = \frac{2p^2}{2\pi} \frac{d\sigma}{dt}$$

$$\simeq 12e^{-3.4(1-\cos\theta)} \text{ mb/sr} . \qquad (6.1)$$

The transformation from center of mass to laboratory angles at small angles is given by

$$\frac{d\theta_{c.m.}}{d\theta_{lab}} \simeq 2\gamma_{c.m.} , \qquad (6.2)$$

where $\gamma_{c.m.}$ is the Lorentz contraction factor for the c.m. frame. The forward angle N-N cross section at 800 MeV is thus

$$\frac{d\sigma_{NN}}{d\Omega_{lab}} \simeq 70e^{-3.4[1-\cos(2.39\theta_{lab})]} \text{ mb/sr} .$$

The total nucleon-nucleon cross section was taken as $\sigma_T = 40$ mb, which is slightly less than σ_T for free nucleon-nucleon scattering to account for the Pauli blocking. The calculated effective number of particles is given in Table I. For the parameters in the scattering operator, Eq. (4.2) we obtained $z_0 = -0.6$ fm and $a_0 = 0.4$ fm.

In Fig. 3 the calculated angular distributions are compared with the 800 MeV (p,p') data from Moss et al.[5] The curve I corresponds to the solu-
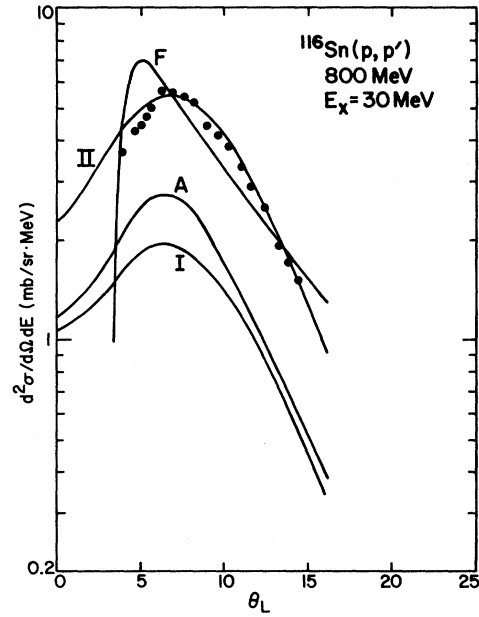
FIG. 3. The experimental (Ref. 5) angular distribution for 800 MeV (p,p') on ^{116}Sn at an excitation energy of 30 MeV is compared with some calculations; curve F gives the Fermi gas model prediction; curve I and II are calculated from Eq. (4.4), where II gives the cross section leading to unbound states and I that for pure knockout. Curve A gives the analytic solution, Eqs. (5.3), (5.5), and (5.8) using $C = 1.7$ fm^2.

tion of Eq. (4.4) in which it has been required that a particle is knocked out from the surface, $k_z'^2 > 0$, while for curve II the less restrictive condition is imposed that the particle scatters to unbound states. The quasielastic knockout process explains only about half of the continuum cross section. The data are well reproduced by curve II. For semi-infinite matter, the difference between the curves I and II corresponds to the single step cross section leading to states for which the momentum component parallel to the surface is large. For finite nuclei the momentum parallel to the surface corresponds to angular momentum. Because of the centrifugal barrier these states have a relatively long lifetime and might eventually decay by particle emission. The angular distribution of the emitted particle will be clearly distinct from that for the direct knockout process. By measuring angular correlations one could thus differentiate between these two processes.

In the analytic solution only the scattering to continuum states has been considered, and it should therefore be compared with curve I to which it indeed gives a fair approximation. In the analytic solution the blocking factor is calculated from Eq. (4.15) using $C = 1.7$ fm^2.

The predictions following from the Fermi gas model are also given in Fig. 3. In this model the cross section vanishes for angles smaller than 3.3° which seems to be in contradiction with the data. For angles larger than 7° the cross sections calculated in the Fermi gas model and the semi-infinite slab model are comparable.

A typical energy spectrum is shown in Fig. 4. This single step excitation to unbound states (curve II) accounts for the measured cross section above an excitation energy of 25 MeV. Only at the very high energies, $E_x > 45$ MeV the major part of the cross section is formed by direct knockout. It would be interesting to study experimentally the fraction of direct knockout as a function of energy to better understand the total reaction strength.

B. 200 MeV (p,n)

The formalism developed in this paper is, in principle, also applicable to the continuum part of the spectrum observed in the (p,n) reaction. In Fig. 5 the experimental angular distribution observed in 200 MeV (p,n) (Ref. 7) is shown. At 200 MeV the total proton-nucleon cross section is only $\sigma_T = 25$ mb/sr (Ref. 8) if we include the effects of Pauli blocking. Owing to this much smaller total
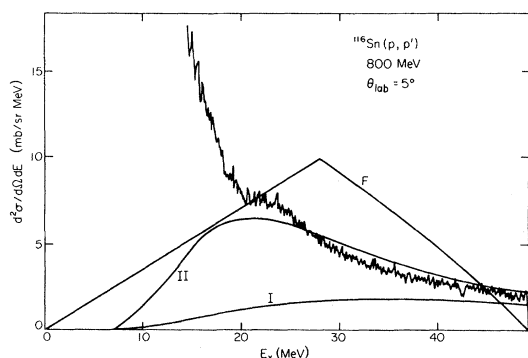
cross section, the effective number of nucleons is about a factor of 2 larger than for 800 MeV protons (see Table I). In the case of the (p,n) reaction we are, however, interested in the effective number of neutrons participating in the scattering process,

$$N_{eff}(p,n) = N_{eff}\sigma_{pn}/(\sigma_{pn}+\sigma_{pp}) , \qquad (6.4)$$

which is about half as large as N_{eff}. Since the charge exchange cross section at forward angles is about $\frac{5}{7}$ of the 800 MeV cross section, we expect that for the same momentum transfer the cross section for (p,n) at 200 MeV is somewhat smaller than for (p,p') at 800 MeV. Experimentally this is indeed the case for $q \geq \frac{1}{2}k_F$. Owing to the smaller total cross section the penetration depth of the proton in the nucleus is much larger and is reproduced by taking $z_0 = -1.05$ fm and $a_0 = 0.7$ fm in the scattering operator Eq. (4.2). For angles larger than 14° both the calculation II and the Fermi gas model account for the observed cross section.

At angles smaller than 8° the calculations underpredict the data. This seems to indicate that the amount of blocking is considerably overestimated. For zero blocking the cross section would be constant at small angles. By decreasing the blocking, however, the cross section at small energy losses
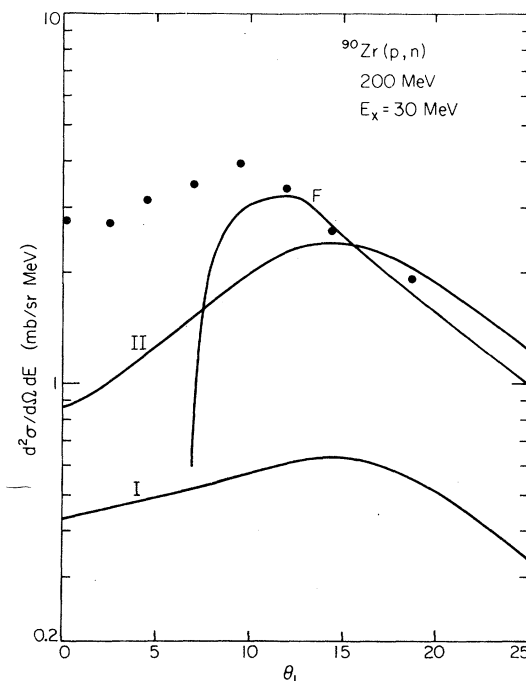
FIG. 4. Experimental (Ref. 5) and calculated energy spectrum for 800 MeV (p,p') on ^{116}Sn at 5° lab angle. The curve labels have the same meaning as in Fig. 2. Below an energy of 10 MeV the experimental spectrum is truncated.

FIG. 5. Same as Fig. 2 for 200 MeV (p,n) on ^{90}Zr[7] at an excitation energy of 30 MeV.

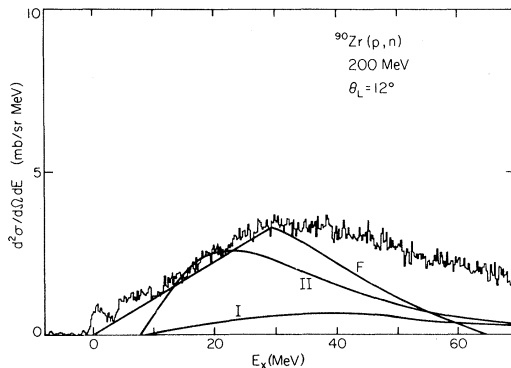FIG. 6. Same as Fig. 3 for 200 MeV (p,n) on ^{90}Zr[7] at 12° lab angle.

will be overpredicted (see Fig. 6). Related to this is the excitation of the Gamow-Teller (GT) resonance. The operator exciting the GT does not change the orbital angular momentum of the particles and so would be Pauli blocked in our treatment. Experimentally, only a small fraction of this strength has been located in peaks and the remaining, about 40 mb/sr at forward angles,[9] could be hidden in the continuum part of the spectrum. This missing strength can easily explain the experimental cross section at 0°. The $L = 0$ angular distribution for the GT strength is, however, strongly forward peaked and it is therefore not possible to use this to explain the difference between experiment and calculation at all angles smaller than 8°. A contribution from higher L transfer would be necessary. It would be interesting to measure the background in an $N = Z$ nucleus to see if the lack of Pauli blocking for the neutron excess is really responsible for the small angle cross section. The forward angles cross section will also be affected by the optical distortion of the projectile wave function. Our treatment deals with the absorption of the projectile but not with the real part of the optical potential. To study the effect of the distortion we compared distorted wave Born approximation calculations for the inelastic cross section with and without distortion from the real potential. The effect on the ratio of the zero degree to the maximum cross sec-

tion is inconsequential for 30 MeV energy loss. At higher excitations ($E_x \gtrsim 50$ MeV) a significant part of the cross section could come from two or more step contributions.

VI. SUMMARY AND CONCLUSIONS

We have calculated the single-collision inelastic scattering cross section in the Fermi gas model and the semi-infinite slab model. For large momentum transfer, $q \geq k_F$ and $E \geq 20$ MeV, the predictions following from these models are similar and agree with experiment. For low momentum transfer the situation is less clear. The sharp drop in cross section, predicted in the Fermi gas at $q < k_F/2$, is not seen in the data. The semi-infinite slab model has less of a drop at small q, and agrees with the 800 MeV (p,p') data. However, the model underpredicts the 200 MeV (p,n) cross section.

The semi-infinite slab cross section can be divided into two parts, depending on whether the nucleon is bound or free in the z direction. We found that most of the strength comes from the z-bound wave functions. In a spherical geometry, the z-bound wave functions correspond to orbitals that are below the centrifugal barrier. It is these centrifugally confined orbits that give the major contribution to the collective state response, e.g., the giant quadrupole. We should therefore be cautious in comparing our continuum cross section with the experimental "background" cross section.

On the experimental side, the prediction that most of the strength goes to centrifugally confined excitations can be tested by looking for direct knockout, e.g., $(p,2p)$. This should be weak for excitation energies $\lesssim 35$ MeV.

[1]H. C. Chiang and J. Hüfner, Nucl. Phys. A349, 466 (1980).

[2]R. J. Glauber and G. Matthiae, Nucl. Phys. B21, 135 (1970).

[3]J. Lindhard, K. Dan. Vidensk. Selsk. Mat. Fys. Medd. 28, No. 8 (1954).

[4]O. Benary, L. Price, and G. Alexander, Lawrence Berkeley Laboratory Report UCRL-20000 NN.

[5]J. Moss (private communication).

[6]C. W. de Jager, H. de Vries, and C. de Vries, At. Data Nucl. Data Tables <u>14</u>, 479 (1974).

[7]C. Gaarde, J. Rapaport, T. N. Taddeucci, C. D. Goodman, C. C. Foster, D. E. Bainum, C. A. Goulding, M. B. Greenfield, D. J. Horen, and E. Sugarbaker, Nucl.

Phys. <u>A369</u>, 258 (1981); and T. N. Taddeucci (private communication).

[8]W. O. Lock and D. F. Measday, *Intermediate Energy Nuclear Physics* (Methuen, London, 1970).

[9]G. F. Bertsch, Nucl. Phys. <u>A354</u>, 157 (1981).